# Improved Sensitivity and Resolution in $^1H-^{13}C$ NMR Experiments of RNA

**Bernhard Brutscher,‡ Jérôme Boisbouvier,‡ Arthur Pardi,§ Dominique Marion,‡ and Jean-Pierre Simorre*,‡**

*Contribution from the Institut de Biologie Structurale, Jean-Pierre Ebel C.N.R.S.-C.E.A. 41, Avenue des Martyrs, 38027 Grenoble Cedex, France, and Department of Chemistry and Biochemistry, University of Colorado, Boulder, Colorado, 80309-0215*

*Received August 10, 1998. Revised Manuscript Received September 29, 1998*

**Abstract:** NMR studies of the structure and dynamics in RNA are greatly facilitated by the use of $^{13}C$-labeled molecules and $^1H-^{13}C$ correlation experiments. We demonstrate here that spin-state selective $^{13}C$ frequency editing yields greatly improved sensitivity and resolution in $^1H-^{13}C$ correlation spectra of RNA. A sensitivity enhanced version of the previously introduced TROSY sequence (Pervushin et al., *Proc. Natl. Acad. Sci. U.S.A.* **1997**, *94*, 12366−12371) is proposed, which offers a $\sqrt{2}$ signal enhancement. When compared to a sensitivity enhanced HSQC sequence an up to 3-fold increase in both the sensitivity and resolution is observed for the base carbons in a 15% $^{13}C$-labeled 33-mer RNA at a magnetic field strength of 14.1 T. This increase results from the relaxation interference between the $^{13}C$ chemical shielding anisotropy (CSA) and the $^1H-^{13}C$ dipolar interaction, as well as the simultaneous detection of $^1H$ and $^{13}C$ steady-state polarizations. Simulations indicate that the enhancement effect is maximal at currently available magnetic field strengths ($\leq$18.8 T). It is further shown that the recording of a pair of complementary TROSY experiments, denoted $H^{(\alpha)}$- and $H^{(\beta)}$-TROSY allows the accurate measurement of $^1H-^{13}C$ one-bond coupling constants from the cross-peak positions in the two spectra. An extension of the TROSY sequence is presented for recording high resolution 3D $^{13}C$-edited NOESY spectra.

## Introduction

The introduction of methods for isotope labeling ($^{13}C$, $^{15}N$) of RNA has allowed the determination of a large number of three-dimensional (3D) structures in the past several years. Novel $^{13}C$ and $^{15}N$ heteronuclear experiments developed for RNA have greatly facilitated the assignment process and increased the number of assigned NOE connectivities.[1] For larger RNAs, sequential assignments are still mainly based on through-space NOEs between adjacent base and sugar protons[2] detected in 3D NOESY-HSQC-type experiments, due to the limited sensitivity of the through-bond HCP experiments[3]. A major problem in resonance assignment and extraction of structural constraints in RNAs remains the poor spectral resolution of $^1H-^{13}C$ correlation spectra, resulting from short $^1H$ and $^{13}C$ transverse relaxation times and homonuclear $^{13}C-^{13}C$ scalar couplings. Recently, selective and partial deuteration of RNA molecules were proposed to reduce the proton line widths and to simplify the analysis of $^{13}C$-edited NOESY spectra.[4,5] While this approach is very promising, it does not solve the severe overlap problems in the $^{13}C$ frequency dimension.

There are often a rather limited number of NOE-based internucleotide distance constraints due to the elongated structure and the low density of protons in RNAs. Additional structural information is becoming available from magnetic field alignment effects, induced by a slightly anisotropic magnetic susceptibility tensor of the RNA molecule itself or by steric hindrance of the molecules in an oriented liquid crystalline medium.[6] Residual dipolar couplings or chemical shift variations induced by the field alignment are directly related to the relative orientation of nuclear vectors with respect to a molecule-fixed coordinate system, thus providing structural information which is complementary to NOEs or *J* couplings.[7] High resolution and high sensitivity $^1H-^{13}C$ correlation spectra are required for the accurate measurement of residual dipolar couplings or chemical shift variations.

It has long been recognized[8] that the cross-correlation of chemical shielding anisotropy (CSA) and dipolar interactions causes a differential relaxation effect of the two lines of a peak doublet in a scalar coupled two-spin system. Selection of only the narrow line by an appropriate pulse sequence leads to a gain in spectral resolution and in favorable cases also yields an

* Correspondence author. E-mail: jps@rmn.ibs.fr.
‡ Institut de Biologie Structurale.
§ University of Colorado.

(1) (a) Pardi, A. *Methods Enzymol*. **1995**, *261*, 350−380. (b) Dieckman, T.; Feigon, J. *J. Biomol. NMR* **1997**, *9*, 259−272.
(2) Nikonowicz, E. P.; Pardi, A. *J. Mol. Biol.* **1993**, *232*, 1141−1156.
(3) (a) Marino, J. P.; Schwalbe, H.; Anklin, C.; Bermel, W.; Crothers, D. M.; Griesinger, C. *J. Biomol. NMR* **1995**, *5*, 87−92. (b) Wijmenga, S. S.; Heus, H. A.; Leeuw, H. A.; Hoppe, H. A. E.; van der Graaf, M.; Hilbers, C. W. *J. Biomol. NMR* **1995**, *5*, 82−86.
(4) (a) Tolbert, T. J.; Williamson, J. R. *J. Am. Chem. Soc*. **1996**, *118*, 7929−7940. (b) Tolbert, T. J.; Williamson, J. R. *J. Am. Chem. Soc*. **1997**, *119*, 12100−12108.
(5) (a) Nikonowicz, E. P.; Michnicka, M.; DeJong, E. *Nucleic Acids Res*. **1997**, *25*, 1390−1396. (b) Nikonowicz, E. P.; Michnicka, M.; DeJong, E. *J. Am. Chem. Soc*. **1998**, *120*, 3813−3814.
(6) (a) Tjandra, N.; Bax, A. *Science* **1997**, *278*, 1111−1114. (b) Hansen, M. R.; Rance M.; Pardi, A. *J. Am. Chem. Soc*., in press; (c) Hansen, M. R.; Mueller, L., Pardi, A., submitted.
(7) (a) Prestegard, J. H. *Nature Struct. Biol*. **1998**, *5*, 517−522. (b) Tjandra, N.; Omichinski, J. G.; Gronenborn, A. M.; Clore, G. M.; Bax, A. *Nat. Struct. Biol*. **1997**, *4*, 732−738.
(8) (a) Werbelow, L. G.; Grant, D. M. *Adv. Magn. Reson*. **1977**, *9*, 189−299. (b) Guéron, M., Leroy, J. L., Griffey, R. H. *J. Am. Chem. Soc*. **1983**, *105*, 7262−7266.

10.1021/ja982853l CCC: $15.00 
Published on Web 11/10/1998

increase in sensitivity. The enhancement effect depends mainly on the CSA tensor orientation and magnitude, the internuclear distance, and the magnetic field strength, $B_0$. Recently, several experimental techniques for spin-state selective spectroscopy using exclusively nonselective radio frequency pulses have been developed, TROSY,[9] $S^3E$,[10] IPAP,[11] and HSQC-$\alpha/\beta$.[12] Thus far, applications have focused on uniformly $^{13}C$,$^{15}N$-labeled proteins to record $^1H-^{15}N$ correlation spectra,[9] acquisition of HCCH-COSY experiments involving aromatic side chains,[13] or measurement of coupling constants.[10,11,14] As recently pointed out by Pervushin et al.,[13] spin-state selective spectroscopy offers the additional advantage of simultaneous excitation and detection of $^1H$ and $^{13}C$ (or $^{15}N$) steady-state polarizations. This is especially useful in the case of RNA molecules where the $^1H$ spin−lattice relaxation time constants $T_1$ are significantly longer than the corresponding $^{13}C$ time constants.

Here we show that, in the case of RNA, spin-state selective $^1H-^{13}C$ correlation experiments yield spectra with greatly improved sensitivity and resolution in the $^{13}C$ frequency dimension as compared to standard correlation techniques. The resolution improvement obtained in $^1H-^{13}C$ correlation maps of RNA is essential for resonance frequency assignment and the extraction of structural constraints in larger RNAs. This methodology is demonstrated for the measurement of $^1H-^{13}C$ coupling constants and $^1H-^1H$ NOEs in a 33-mer fractionally $^{13}C$-labeled RNA.

## Methods

**Elimination of Homonuclear $^{13}C-^{13}C$ Scalar Couplings.** Homonuclear $^{13}C-^{13}C$ scalar couplings increase the apparent line widths and lower the resolution in the $^{13}C$ dimension of uniformly $^{13}C$-labeled RNAs. There are two different approaches that can be used to eliminate these couplings, (1) constant time (CT) evolution where the time is an integral multiple of $1/J_{CC}$ or (2) random 10−20% $^{13}C$ labeling of the RNA sample. In both cases the increased spectral resolution is accompanied by a significant loss of sensitivity, which makes it very important to develop more sensitive correlation techniques. To evaluate the respective advantages of the two approaches for studies of RNA, the following points need to be considered: (i) there is a large variation in the size of the homonuclear $J_{CC}$ coupling constants in RNA, with one-bond coupling constants of about 40 Hz for carbons in the sugar ring, whereas these couplings vary between 50 and 85 Hz in the bases. Additionally, long range (two- and three- bond) scalar $J_{CC}$ couplings up to 12 Hz are present. This wide range of coupling constants makes it impossible to simultaneously optimize the constant time delay for all C−H groups; (ii) in the CT approach, the spectral resolution is limited by the choice of the constant time delay, whereas in the fractional $^{13}C$-labeling approach, it can be adjusted to the particular experimental requirements; (iii) for relatively small RNAs, sensitivity will be higher for the CT approach. However, as the molecular size increases, the sensitivity advantage will be shifted toward the fractional $^{13}C$-labeling approach.

For these reasons, we chose to use a 15% $^{13}C$-labeled RNA sample. All experiments are demonstrated on a 33-mer RNA in a 1:1 complex with unlabeled theophylline.[15] The RNA was dissolved in a buffer of 20 mM sodium phosphate (pH 6.8), 30 mM NaCl, 2 mM $MgCl_2$ in $D_2O$ at a sample concentration of about 1 mM. Theophylline was then added to the solution to form a 1:1 complex with the RNA. Data were recorded on Bruker AMX 600 and DMX 800 spectrometers at a sample temperature of 298 K. Processing was achieved using the FELIX program version 97.0 (Molecular Simulations Inc.).

**Sensitivity-Enhanced 2D TROSY and 3D TROSY-NOESY Pulse Sequences.** The pulse schemes employed for the 2D $^1H-^{13}C$ correlation experiments and 3D $^{13}C$-edited NOESY experiments are shown in Figure 1A and B, respectively. The sequences are based on the recently introduced concept[9] of transverse-relaxation optimized spectroscopy (TROSY). The central part of the TROSY sequence is a spin-state selective coherence transfer between the two scalar coupled spins $^{13}C$ and $^1H$. In product operator notation[16] the coherence transfer pathway can be written as $C_{x,y}^{(\beta)} \rightarrow H_{x,y}^{(\alpha)}$, where $C_x^{(\beta)}$ and $H_x^{(\alpha)}$ represent single-transition operators of the carbon and proton spins, respectively. The superscripts ($\alpha$) and ($\beta$) indicate the spin-state of the coupling partner following a commonly used sign convention.[17] Spin-state selection is obtained by the pulse sequence in Figure 1 and a four-step phase cycle as described in the figure caption. The spin-state-selective coherence transfer pathway can be altered to $C_{x,y}^{(\beta)} \rightarrow H_{x,y}^{(\beta)}$ by a 180° phase shift of $\psi_2$ (Figure 1A and B). To distinguish between the two experiments we will refer to them as $H^{(\alpha)}$-TROSY and $H^{(\beta)}$-TROSY.

Both orthogonal coherences $C_x^{(\beta)}$ and $C_y^{(\beta)}$, present at the end of $t_1$, are transferred simultaneously into detectable $^1H$ coherences. A sensitivity-enhanced version of the TROSY sequence is obtained by separately storing the four repetitions of the experiment. This acquisition scheme and thus the data processing are conceptually identical to other phase-modulated detection techniques (echo−antiecho) in indirect frequency dimensions of NMR experiments.[18] The four experiments are then combined as indicated in Figure 1 to reconstruct the real (*Real*) and imaginary (*Im*) parts of the free induction decay (FID) in $t_1$ ($^{13}C$). Since the real and imaginary parts of the FID in $t_1$ are detected in orthogonal components of the complex FID in $t_2$ ($^1H$), an additional 90° phase shift has to be applied for each imaginary $t_1$ point in the $t_2$ dimension. This version of TROSY offers a $\sqrt{2}$ increased sensitivity with respect to the originally proposed pulse scheme.[19]

An extension of the TROSY sequence, adding a second incremented delay ($t_2$) for $^1H$ frequency labeling and a NOE mixing period (Figure 1B), allows the recording of 3D $^{13}C$-edited NOESY spectra. This specific arrangement, TROSY-NOESY instead of NOESY-TROSY, is preferred, because it allows the combined use of $^1H$ and $^{13}C$ initial polarizations as discussed below. The $\sqrt{2}$ sensitivity enhancement as described for the 2D TROSY experiment of Figure 1A (phase-modulated detection in $t_1$) is conserved in this 3D TROSY−NOESY version. After the NOE mixing and the final 90° $^1H$ pulse, the spin system is described by the product operator $H_y = H_y^{(\alpha)} + H_y^{(\beta)}$. To avoid $J_{CH}$ splittings, the $^{13}C$ spins are broadband-decoupled during detection.

**Simultaneous Excitation and Detection of $^1H$ and $^{13}C$ Steady-State Polarization.** Most heteronuclear correlation experiments employed for the study of biomolecules use an initial INEPT transfer step.[20] The INEPT sequence simultaneously transfers proton polarization $H_z$ into heteronuclear antiphase coherence $2C_xH_z$ and carbon polarization $C_z$ into in-phase coherence $C_x$. In the standard pulse sequences only the antiphase coherence is further transferred into an observable NMR signal. The experiments of Figure 1 A and B also use an initial INEPT step for spin excitation. The spin-state-selective coherence transfer realized by the TROSY sequence simultaneously converts both proton and carbon initial polarization into a observable NMR signal. This

(9) Pervushin, K.; Riek, R.; Wider, G.; Wüthrich, K. *Proc. Natl. Acad. Sci. U.S.A.* **1997**, *94*, 12366−12371.

(10) (a) Meissner, A.; Duus, J.; Sørensen, O. W. *J. Magn. Reson.* **1997**, *128*, 92−97. (b) Meissner, A.; Duus, J.; Sørensen, O. W *J. Biomol. NMR* **1997**, *10*, 89−94.

(11) Ottiger, M.; Delaglio, F.; Bax, A. *J. Magn. Reson.* **1998**, *131*, 373−378.

(12) Anderson, P.; Nordstrand, K.; Sunnerhagen, M.; Liepinsh, E.; Turovskis, I.; Otting G. *J. Biomol. NMR* **1998**, *11*, 445−450.

(13) Pervushin, K.; Riek, R.; Wider, G.; Wüthrich, K. *J. Am. Chem. Soc.* **1998**, *120*, 6394−6400.

(14) Meissner, A.; Schulte-Herbrüggen, T.; Sørensen, O. W. *J. Am. Chem. Soc.* **1998**, *120*, 3803−3804.

(15) Zimmermann, G. R.; Jenison, R. D.; Wick, C. L.; Simorre, J.-P.; Pardi, A. *Nat. Struct. Biol.* **1997**, *4*, 644−649.

(16) Sørensen, O. W.; Eich, G. W.; Levitt, M. H.; Bodenhausen, G.; Ernst, R. R. *Prog. Nucl. Magn. Reson. Spectrosc.* **1983**, *16*, 163−192.

(17) Cavanagh, J.; Fairbrother, W. J.; Palmer, A. G., III; Skelton, N. J. *Protein NMR Spectroscopy*; Academic Press Inc.: San Diego, 1996.

(18) Palmer, A. G., III; Cavanagh, J.; Wright, P. E.; Rance, M. *J. Magn. Reson.* **1991**, *93*, 151−170.

(19) A sensitivity-enhanced TROSY experiment has been published during the publication procedure of this manuscript by Andersson, P.; Annila, A.; Otting, *J. Magn. Reson.* **1998**, *133*, 364−367.

(20) Morris, G. A.; Freeman, R. *J. Am. Chem. Soc.* **1979**, *101*, 760−762.

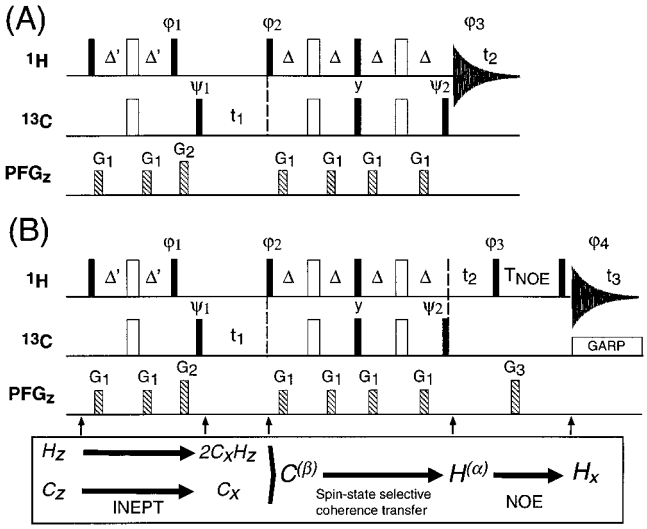


**Figure 1.** Pulse sequences for (A) 2D TROSY and (B) 3D TROSY-NOESY experiments. The relevant coherence transfer pathways are indicated on the bottom. Thin bars represent 90° and open bars 180° rf pulses. Composite $^{13}C$ 180° pulses are used for broadband spin inversion ($90°_x$, $240°_y$, $90°_x$) and refocusing ($59.4°_x$, $298°_{-x}$, $59.4°_x$). All pulses are applied along the $x$ axis unless indicated. The transfer delays $\Delta$ and $\Delta'$ are adjusted to 1/4 $J_{CH}$, taking into account the different relaxation times of the involved coherences. In the present case they were set to $\Delta = 1.3$ ms, $\Delta' = 1.0$ ms. In the TROSY experiment no $^{13}C$ decoupling is applied during detection and, in the TROSY-NOESY experiment $^{13}C$ decoupling was achieved using GARP with an rf field strength of $|\gamma B_1|/2\pi = 3$ kHz. Pulsed field gradients along the $z$ axis ($PFG_z$) were applied as indicated for coherence transfer pathway selection. The gradient strength was approximately 20 G/cm, and the pulse lengths were set to $G_1 = 300$ ms, $G_2 = 900$ ms, and $G_3 = 400$ ms, followed by a recovery delay of 300 ms. For quadrature detection and spin-state selection in $t_1$, four repetitions ($E_1$ to $E_4$) of the experiment are recorded with the following phase settings for $H^{(\beta)}$-TROSY: $E_1$: $\varphi_1 = y$; $\varphi_2 = y$; $\psi_1 = -x, x$; $\psi_2 = x$, $\varphi_3 = x, -x$; $E_2$: $\varphi_1 = y$; $\varphi_2 = y$; $\psi_1 = -y,y$; $\psi_2 = x$, $\varphi_3 = y, -y$; $E_3$: $\varphi_1 = y$; $\varphi_2 = -y$; $\psi_1 = -x, x$; $\psi_2 = -x$, $\varphi_3 = x, -x$;. $E_4$: $\varphi_1 = y$; $\varphi_2 = -y$; $\psi_1 = -y,y$; $\psi_2 = -x$, $\varphi_3 = y, -y$; The $H^{(\alpha)}$-TROSY version is obtained by a 180° phase shift of $y_2$ in all four experiments. To reconstruct the real and imaginary parts of the FID in $t_1$, the four recorded and separately stored experiments are combined as follows: *Real* $(t_1) = -E_1 + E_2 + E_3 + E_4$: *Im* $(t_1) = E_1 - E_2 + E_3 + E_4$. Before Fourier transformation, the imaginary parts *Im* $(t_1)$ are phase shifted by 90° along the $t_2$ ($^1H$) dimension. For the 3D TROSY-NOESY experiment, four repetitions ($E_1-E_4$) are again recorded and stored separately for each $t_1$ increment with the following phase cycling: $E_1$: $\varphi_1 = y$; $\varphi_2 = y$; $\psi_1 = -x, x$; $\psi_2 = x$, $\varphi_3 = x$, $\varphi_4 = x, -x$; $E_2$: $\varphi_1 = y$; $\varphi_2 = y$; $\psi_1 = -y,y$; $\psi_2 = x$, $\varphi_3 = y$, $\varphi_4 = x, -x$; $E_3$: $\varphi_1 = y$; $\varphi_2 = -y$; $\psi_1 = -x, x$; $\psi_2 = -x$, $\varphi_3 = x$, $\varphi_4 = x, -x$; $E_4$: $\varphi_1 = y$; $\varphi_2 = -y$; $\psi_1 = -y,y$; $\psi_2 = -x$, $\varphi_3 = y$, $\varphi_4 = x, -x$; The four experiments are combined and phase-shifted as in the 2D TROSY. For quadrature detection in $t_2$, time proportional phase incrementation of $\varphi_3$ is applied according to STATES-TPPI.[37]

can be rationalized by expressing the single-transition operators $C_x^{(\alpha)}$ and $C_x^{(\beta)}$ in terms of in-phase and antiphase transverse coherences $C_x$ and $2C_xH_z$, $C_x^{(\alpha)} = {}^1/_2(C_x - 2C_xH_z)$ and $C_x^{(\beta)} = {}^1/_2(C_x + 2C_xH_z)$. Therefore, if a $C^{(\alpha)}$ or $C^{(\beta)}$ spin state is selected after the $^{13}C$ frequency-labeling period ($t_1$), both coherence transfer pathways will contribute to the detected signal as indicated at the bottom of Figure 1 for the $H^{(\alpha)}$-TROSY version. Depending on the relative sign between in-phase and antiphase coherences at the end of the INEPT sequence, either the $C^{(\alpha)}$ or the $C^{(\beta)}$ spin state is selectively enhanced. Experimentally this enhancement effect is controlled by the phase setting of the proton 90° pulse ($\varphi_1$). The experiments of Figure 1A and B have been designed for sensitivity enhancement and selection of the $C^{(\beta)}$ spin state.

To assess the sensitivity gain arising from the simultaneous excitation and detection of $^1H$ and $^{13}C$ steady-state polarizations in the TROSY, we define an enhancement factor relative to a standard correlation experiment, as $\lambda_1$

$$\lambda_1 = \frac{I_0(H_z) + I_0(C_z)}{Max\{I_0(H_z), I_0(C_z)\}} \tag{1}$$

where $I_0(H_z)$ and $I_0(C_z)$ represent the signal intensity originating from the proton and carbon initial spin polarizations, respectively. This factor allows a valid comparison of different NMR correlation experiments. It takes into account that in the case of a higher $^{13}C$ than $^1H$ initial magnetization, the TROSY experiment should be compared with an experiment starting only with $^{13}C$. Note that this definition of $\lambda_1$ implies that the maximal sensitivity gain is a factor of 2 ($\lambda_1 \leq 2.0$).

**CSA−Dipolar Cross-Correlated Relaxation Effects.** An additional gain in spectral resolution and thus in sensitivity is obtained from the constructive use of CSA−dipolar relaxation interference in a scalar-coupled $^{13}C-^1H$ two-spin system. In the $^{13}C$ frequency dimension the two components of the $J$-doublet are affected in a different way; one line is narrowed and the other one is broadened by the relaxation interference.

To assess the gain in spectral resolution when selecting only the narrow line of the doublet (corresponding to the $C^{(\beta)}$ transition in the present case) with respect to a $^1H$ decoupled spectrum, we define a second enhancement factor $\lambda_2$

$$\frac{1}{\lambda_2} = R(C_x^{(\beta)})/R(C_x) = 1 + \frac{\Gamma_{CSA,DD}}{\overline{R_x^{DD}} + R_x^{CSA}} \tag{2}$$

In the $t_1$ dimension of HSQC- and TROSY-type experiments, the $^{13}C$ coherences decay with the rate constants $R(C_x)$ and $R(C^{(\beta)})$, respectively. $\overline{R_x^{DD}} = (R^{DD}(C_x) + R^{DD}(2C_xH_z))/2$ represents the dipolar contribution, $R_x^{CSA}$ the CSA contribution and $\Gamma_{CSA,DD}$ the relaxation interference between these two mechanisms. In a Lipari and Szabo model of the molecular dynamics,[21] assuming an isotropic overall rotational tumbling in the slow motion regime ($\tau_c\omega_o \gg 1$), and isotropic local fluctuations in the extreme narrowing limit ($\tau_{int}\omega_o \ll 1$), the enhancement factor $\lambda_2$ becomes independent of the motional parameters ($\tau_c$, $S^2$, $\tau_{int}$) and is given by the following simple relation:[22]

$$\frac{1}{\lambda_2} = 1 - \frac{12\xi_{DD}\omega_C\Delta\sigma^*}{9\xi_{DD}^2 + 4\omega_C^2(\overline{\Delta\sigma})^2} \tag{3}$$

with the dipolar constant $\xi_{DD} = \mu_0/4\pi\ \gamma_C\gamma_H/\langle R_{C-H}^3\rangle\ h/2\pi$, and $^{13}C$ Larmor frequency $\omega_c = \gamma_C B_0$. $\gamma_C$ and $\gamma_H$ are the gyromagnetic ratios of $^{13}C$ and $^1H$, h is Planck's constant, and $\mu_o$ is the magnetic field constant. The $^{13}C$ CSA is described by the two relaxation relevant constants $\overline{\Delta\sigma} = \sqrt{\sigma_x^2+\sigma_y^2-\sigma_x\cdot\sigma_y}$ and $\Delta\sigma^* = P_2(\cos\theta^{xd})\sigma_x + P_2(\cos\theta^{yd})\sigma_y$, with $\sigma_x = \sigma_{xx} - \sigma_{zz}$ and $\sigma_y = \sigma_{yy} - \sigma_{zz}$. $\sigma_{xx}$, $\sigma_{yy}$, $\sigma_{zz}$ are the principal values of the CSA tensor, $\theta^{xd}$ and $\theta^{yd}$ are the angles between the internuclear $^{13}C-^1H$ vector and the principal axes $x$ and $y$ of the CSA tensor, and $P_2(x)$ is the Legendre polynomial $P_2(x) = (3x^2 - 1)/2$.

The line narrowing effect depends mainly on the $B_0$ field strength and the $^{13}C$ CSA tensor orientation and magnitude. It can be seen from eq 3 that a maximal effect is expected for axially symmetric CSA tensors with the principal axis parallel to the C−H bond vector ($\overline{\Delta\sigma} = \Delta\sigma^*$) and where the dipolar interaction is of the same magnitude as the CSA interaction ($\xi_{DD} = \omega_C\overline{\Delta\sigma}$). At this time no experimental or theoretical CSA data are available for carbons in purine or pyrimidine bases. For different benzene derivatives, CSA tensor orientations were reported with one principal axis along the $^{13}C-^1H$ bond vector and a second one orthogonal to the aromatic ring. While the orientations are almost conserved among these systems, large variations in the CSA

(21) (a) Lipari, G.; Szabo, A. *J. Am. Chem. Soc.* **1982**, *104*, 4546−4559. (b) *J. Am. Chem. Soc.* **1982**, *104*, 4559−4570.
(22) Goldman, M. *J. Magn. Reson.* **1984**, *60*, 437−452.

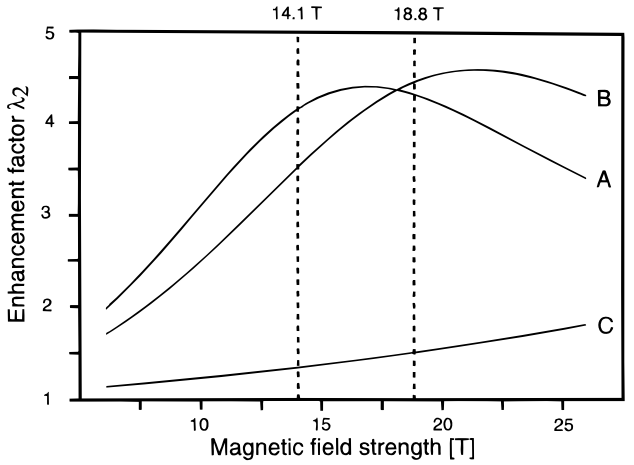


**Figure 2.** Simulations of the enhancement factor $\lambda_2$ as defined in eq 2 are plotted as a function of the magnetic field strength $B_0$. The $^{13}C$ CSA values are: (A) $\overline{\Delta\sigma} = 156$ ppm and $\Delta\sigma^* = 122$ ppm for acetophone ($T = 77$ K),[24] (B) $\overline{\Delta\sigma} = 198$ ppm and $\Delta\sigma^* = 153$ ppm for $\beta$-quinol ($T = 103$ K),[25] and (C) $\overline{\Delta\sigma} = \Delta\sigma^* = 32$ ppm ($T = 273$ K)[26] for an oxygen-bound sugar-ring carbon. The internuclear distance was set to $r_{C-H} = 1.08$ Å.

magnitude are reported. The relaxation relevant parameters $\overline{\Delta\sigma}$ and $\Delta\sigma^*$ vary from 144 to 208 ppm and 122 to 161 ppm, respectively.[23]

The enhancement effect $\lambda_2$ for RNA base carbons as a function of the $B_0$ field strength was estimated using the CSA data for two benzene derivatives measured by solid-state NMR techniques at low temperature. The $B_0$ field dependence calculated using eq 3 for acetophone[24] and $\beta$-quinol[25] are shown in Figure 2A and B, respectively. The two curves show a similar overall behavior, with an enhancement factor of $\lambda_2 =$ 3.5 to $\lambda_2 = 4.5$ at currently available magnetic field strengths of 14.1 or 18.8 T. The maximum is slightly shifted to higher magnetic field strengths in the case of $\beta$-quinol (from 17 to 21.5 T).

In the case of the sugar carbons, a smaller enhancement effect is expected. Solid-state NMR measurements show that chemical shielding anisotropies for sugar carbons are about 5 times smaller than those for aromatic carbons. To simulate the $B_0$ field dependence of $\lambda_2$ for RNA sugar carbons, an axially symmetric CSA tensor was assumed with the principal axis parallel to the C−H bond vector. To get a realistic model for $C_{1'}$ carbons the $\overline{\Delta\sigma}$ value was taken from the measurements on a ring C−H bound to an oxygen: $\overline{\Delta\sigma} = 32$ ppm.[26] The calculated curve is shown in Figure 2C. From the simulations, maximal enhancement factors of $\lambda_2 = 1.3$ and $\lambda_2 = 1.5$ are obtained at 14.1 and 18.8 T, respectively.

The line narrowing effect described above can also lead to a sensitivity gain. The actual gain, however, depends on the choice of acquisition and processing parameters. For very long acquisition times (of several $T_2$), and without application of an apodization function the sensitivity gain is equal to $\lambda_2$. In practice, however, the effective sensitivity gain is somewhat lower, since the acquisition time and the number of scans can be optimized for the different relaxation properties in the two correlation experiments. In summary, an upper limit of the total sensitivity gain $\lambda$ in TROSY with respect to HSQC-type experiments arising from the above-described effects is given by $\lambda \leq (\lambda_1\lambda_2)/2$, where $\lambda_1$ is related to the initial spin polarization, $\lambda_2$ to the spectral resolution enhancement, and the factor of 1/2 to the spin-state selection.

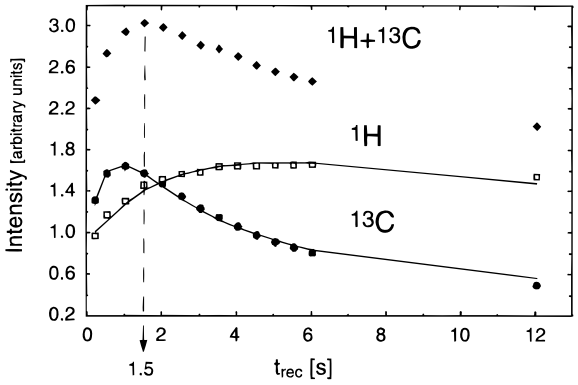


**Figure 3.** Recovery curves of $^1H$ and $^{13}C$ polarization in the 33-mer RNA-theophylline complex. 1D spectra were recorded using the pulse sequence of Figure 1A with $t_1 = 0$ and an experimental time of 30 min per experiment. Destruction of either the $^1H$ or $^{13}C$ polarization was experimentally accomplished by a 90° ($^1H$ or $^{13}C$) pulse−$PFG_z$ purging sequence. The intensities obtained from integration over the spectral regions of the base protons and the $H_{1'}$ sugar protons are normalized for equal noise levels and plotted as a function of the recycle delay $t_{rec}$ for $^1H$ (□) and $^{13}C$ (●) initial polarizations. The experimental intensities, $I(t_{rec})$, were fit to the empirical function $I(t_{rec}) = I_\infty[1 - \exp(-(t_{rec} - t_0)/T_1)]/\sqrt{t_{rec}}$ by optimizing the parameters $I_\infty$ and $T_1$ (solid lines). Whereas in the case of the $^{13}C$ data the fit was accomplished with $t_0 = 0$, an additional parameter $t_0$ was necessary to fit the $^1H$ recovery data. This is most likely due to the multiexponential relaxation behavior of the $^1H$ spins. The calculated $^{13}C$ relaxation time constant $T_1$ has been further corrected to account for a $\{^1H\}^{13}C$ steady-state NOE of 1.25. The sum of $^1H$ and $^{13}C$ steady-state polarizations (◆) is maximal at a recycle delay of 1.5 s.

## Results and Discussion

**Experimental Estimation of $^1H$ and $^{13}C$ Steady-State Polarizations.** Both, $^1H$ and $^{13}C$ polarizations are converted by the TROSY sequence into observable coherences. Since the detected signal is directly proportional to the gyromagnetic ratio $\gamma$ of the excited nucleus, a 25% signal increase is expected for a fully relaxed $^{13}C-^1H$ spin pair in the TROSY experiment with respect to a standard HSQC correlation experiment ($\gamma_H/\gamma_C \approx 4$). An even higher sensitivity gain is expected in the case of nonequilibrium steady-state conditions for molecules where $T_1(^1H) > T_1(^{13}C)$. As compared to proteins and DNA fragments, RNAs exhibit remarkably long $^1H$ $T_1$ relaxation rate constants. In fully protonated or partially deuterated RNAs, proton $T_1$ relaxation times of several seconds are reported,[4,27] much longer than the corresponding $^{13}C$ $T_1$ time constants.

To determine the relative importance of $^1H$ and $^{13}C$ steady-state polarization as a function of the recycle delay in the RNA sample, a series of one-dimensional (1D) TROSY spectra were recorded at 14.1 T $B_0$ field strength by destroying either the $^1H$ or the $^{13}C$ polarization *prior* to the INEPT sequence. The number of scans was adjusted for each 1D experiment to ensure equal measuring times. The 1D spectra were normalized for equal noise levels and integrated over the spectral regions of the base protons and the $H_{1'}$ sugar protons. These integrated intensities, plotted as a function of the recycle delay $t_{rec}$, are shown in Figure 3. Although a multiexponential behavior is expected, the data are consistent with a simple model taking into account effective $T_1$ relaxation times and a $\{^1H\}^{13}C$ NOE (Figure 3). The fitted average relaxation time constants are $T_1(^{13}C) = 0.7$s and $T_1(^1H) = 4.6$ s; thus, $^1H$ longitudinal

(23) Veeman, W. S. *Prog. Nucl. Magn. Reson. Spectr.* **1984**, *16*, 193−235.
(24) van Dongen Torman, J.; Veeman, W. S.; de Boer, E. *J. Magn. Reson.* **1978**, *32*, 49−55.
(25) Matsui, S.; Terao, T.; Saika, A. *J. Chem. Phys.* **1982**, *77*, 1788−1799.
(26) Liu, F.; Phung, C. G.; Alderman, D. W.; Grant, D. M. *J. Am. Chem. Soc.* **1996**, *118*, 10629−10634.
(27) (a) Wang, A. C.; Kim, S. G.; Flynn, P.; Chou, S. H.; Orban, J. Reid, B. *Biochemistry* **1992**, *31*, 3940−3946. (b) Liu, H.; Tonelli, M.; James, T. L. *J. Magn. Reson.* **1996**, Series B, 111, 85−89. (c) Mujeeb, A.; Reynolds, M. A.; James, T. L. *Biochemistry* **1997**, *36*, 2371−2379.

relaxation is, on average, a factor of 7 slower than that for $^{13}C$ in this molecule. The experimental curves indicate an up to 2-fold increase in sensitivity when detecting simultaneously both $^1H$ and $^{13}C$ polarizations, as is done in the TROSY sequence, thus compensating for the loss by a factor of 2 of signal as a result of the selection of either the $C^{(\alpha)}$ or $C^{(\beta)}$ spin states. The maximal sensitivity is obtained at relatively short recycle delays of 1.5 s, which represents the additional advantage of higher repetition rates with respect to experiments starting only with $^1H$ polarization, where a much longer recycle delay is needed ($t_{rec} \approx 5$ s) for optimal sensitivity. This is especially important in high resolution 3D spectra, where it is impractical to have such a long recycle delay.

Similar $^1H$ and $^{13}C$ relaxation time constants[27,28] have been observed for other protonated RNAs. Whereas the $^{13}C$ relaxation time constants observed are comparable to the values measured in proteins of the same size, $^1H$ $T_1$ time constants are always substantially longer; $T_1 > 3$s (for base protons) and $T_1 > 1.5$ s (for sugar protons) have been frequently reported for molecules containing between 20 and 30 nucleotides. In DNA−RNA complexes, the difference in spin−lattice relaxation times between $H_{1'}$ protons in the DNA and RNA strands has been repeatedly observed and ascribed to the lack of $H_{2'}$, which is one of the most efficient relaxation partners for $H_{1'}$ in deoxyribose sugars. For partially deuterated RNAs, the $^1H$ relaxation times are even further increased,[4] whereas the relaxation times of $^{13}C$ bound to $^1H$ remain nearly unchanged. This behavior is due to the different spin interactions involved in the relaxation process. The $^{13}C$ spin−lattice relaxation is dominated by the heteronuclear $^1H-^{13}C$ dipolar interaction, whereas longitudinal $^1H$ spin relaxation is mainly caused by the homonuclear dipolar interactions with other nearby protons. The latter is sensitive to the zero-frequency component of the spectral density of molecular motion and is therefore more efficient than the heteronuclear $^1H-^{13}C$ interaction for spin−lattice relaxation in larger molecules. The proton density, which is lower in RNA than in proteins and is further reduced by deuteration, therefore only alters the efficiency of $^1H$ relaxation.

Simulations of the $^1H$ and $^{13}C$ steady-state polarizations assuming different ratios of relaxation time constants $T_1(^1H)/T_1(^{13}C)$ varying from 3 to 10 have been performed (results not shown). Simultaneous excitation and detection of $^1H$ and $^{13}C$ steady-state polarizations always yields a sensitivity gain in the range of $\lambda_1 = 1.5-2.0$ when compared to experiments starting either from $^1H$ or $^{13}C$ polarization. The results described in the following sections are therefore not limited to this 15% $^{13}C$-labeled RNA but represent a general method for the study of fully protonated or partially deuterated RNAs.

**$^1H-^{13}C$ High-Resolution Correlation Spectra.** Data sets of $H^{(\alpha)}$-TROSY using the pulse sequence of Figure 1A were recorded at 14.1 T $B_0$ field strength (Figure 4B). The delay $\Delta$ of the spin-state selective coherence-transfer step was adjusted in order to optimize the sensitivity of the experiment and to reduce the intensity of undesired doublet components in the $^1H$ frequency dimension. Analysis of the involved coherence transfer pathways reveals that the selected and the residual doublet components are detected with relative intensities of $(\sin^2(2\pi J_{CH}\Delta) + \sin(2\pi J_{CH}\Delta) + 1)/4$ and $(\sin^2(2\pi J_{CH}\Delta) - 1)/2$, respectively. One-bond $J_{CH}$ coupling constants in RNA vary from about 170 Hz for the $C_{1'}$ and $C_{2'}$ sugar carbons to 220 Hz for the $C_8$ carbons in purine bases. Neglecting relaxation effects, for the present choice of $\Delta = 1.3$ ms the transfer efficiency for all C−H pairs in the bases and for the sugar $C_{1'}$ is >96% for the selected and <2.5% for the undesired residual component. Experimentally the intensities of residual peaks were found to be below the noise level even for the most intense correlation peaks.

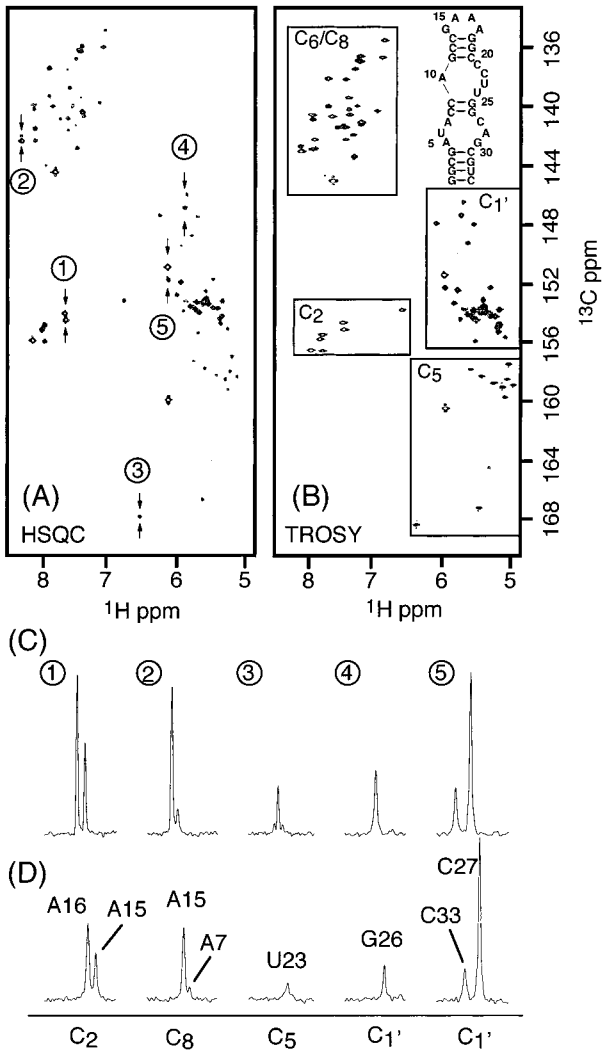


**Figure 4.** Sensitivity-enhanced (A) 2D HSQC and (B) 2D $H^{(\alpha)}$-TROSY spectra of the 15% $^{13}C$-labeled 33-mer RNA−unlabeled theophylline complex. The secondary structure of the RNA is drawn on top of (B). The recycle delay for both experiments was set to 1.5 s. The spectra were recorded at 14.1 T $B_0$ field strength with 1024 ($^1H$) × 256 ($^{13}C$) complex points, spectral widths of 13 ppm ($^1H$) and 60 ppm ($^{13}C$) and a total acquisition time of 12 h per experiment. After multiplication with a squared cosine apodization function in both dimensions, the spectra were zero-filled and Fourier-transformed to final matrixes of 1024 × 1024 points. Note that the $C_5$ and $C_{1'}$ resonances are outside the $^{13}C$ spectral width so they are folded in the spectrum. In addition, $^{13}C$ traces of (C) TROSY and (D) HSQC are shown for C−H groups in different bases and sugars, where the circled numbers represent traces of the cross-peaks indicated in (A) and the resonance assignments of these traces are shown in (D).

For comparison, a sensitivity-enhanced HSQC experiment[18] was performed under the same experimental conditions (Figure 4A). As expected, there is a general increase in sensitivity for the TROSY in all spectral regions of the 2D correlation map. For the aromatic carbons, a significant line narrowing effect is observed, whereas only a small effect is detected for the sugar carbons. $^{13}C$ traces of the $H^{(\alpha)}$-TROSY (Figure 4C) and HSQC (Figure 4D) spectra are plotted for various types of C−H groups. For the $C_{1'}$ sugar carbon of G26 (Peak 4) a sensitivity gain of a factor of $\lambda = 1.6$ and a small resolution enhancement are

(28) Hall, K. B.; Tang, C. *Biochemistry* **1998**, *37*, 9323−9332.

observed. Similar enhancement factors ($\lambda = 1.4$ to 1.8) are measured for other $C_{1'}$ carbons in this RNA. These results are consistent with the CSA−dipolar relaxation interference simulations of Figure 2 and the assumption of an almost equal contribution of $^1$H and $^{13}$C initial polarizations ($\lambda_1 \approx 2$, $\lambda_2 \approx 1.4$) (Figure 3). For nucleotide C27, which is situated in a highly unstructured and flexible part of the molecule,[15] no signal increase is obtained for the $C_{1'}$ carbon (Peak 5). For the base carbons, the sensitivity gain varies from $\lambda = 2.5$ to $\lambda = 3.5$. The highest enhancement factors are obtained for $C_5$ base carbons (Peak 3). As expected from the simulations of Figure 2, a significant line narrowing effect is observed for all base carbons. In the case of $C_5$-U23, one can even distinguish two satellite peaks originating from carbons with one $^{13}$C-labeled neighbor. Nevertheless, the observed line narrowing and sensitivity gain for base carbons are slightly less than what is expected from the CSA−dipolar relaxation interference simulations of Figure 2. Preliminary results on the experimental determination of the two relaxation relevant CSA parameters $\overline{\Delta\sigma}$ and $\Delta\sigma^*$ in purine and pyrimidine bases of RNA (unpublished results) indicate that the model compounds slightly overestimate the enhancement effect.

Inspection of the line widths in the $^1$H dimension shows that the difference between the HSQC and spin-state selective TROSY experiment is less than 10%, indicating a negligible CSA for the $^{13}$C-bound protons in RNA. This finding is consistent with CSA values of $\overline{\Delta\sigma} \leq 5$ ppm, reported in the literature for other aromatic carbon-bound protons.[29]

From the $H^{(\alpha)}$-TROSY spectrum of a 15% $^{13}$C-labeled RNA molecule, it is possible to resolve most of the C−H correlation peaks for aromatic and $C_{1'}$ carbons and many of the other sugar carbons in this RNA. High resolution $^1$H−$^{13}$C correlation maps can be extremely useful in identification of bases with shifted p$K_a$s, metal ion binding sites and unusual dynamics in RNAs.[30] The sensitivity improvement obtained by the TROSY experiments will also aid in the acquisition of $^1$H−$^{13}$C correlation spectra on natural abundance RNA samples. This will be important for preliminary NMR studies on unlabeled molecules to evaluate the feasibility of a specific RNA for structural studies or to optimize the sample conditions.

High resolution $^1$H−$^{13}$C correlation spectra allow the accurate measurement of $^1$H and $^{13}$C resonance frequencies. It is now well-established that chemical shifts, combined with *ab initio* quantum-chemical calculations[31] or a statistical analysis of chemical shift databases,[32] yield valuable information on local structure of proteins. Recently, some attempts have been made to use $^{13}$C and $^1$H chemical shifts for the structure determination of nucleic acids.[33] In addition, the chemical shift variations which are induced by a molecular alignment in the magnetic field[34] can also be related to molecular structure, provided that accurate CSA tensors are available. It is likely that such chemical shift data will become increasingly used in structure calculations of RNA.

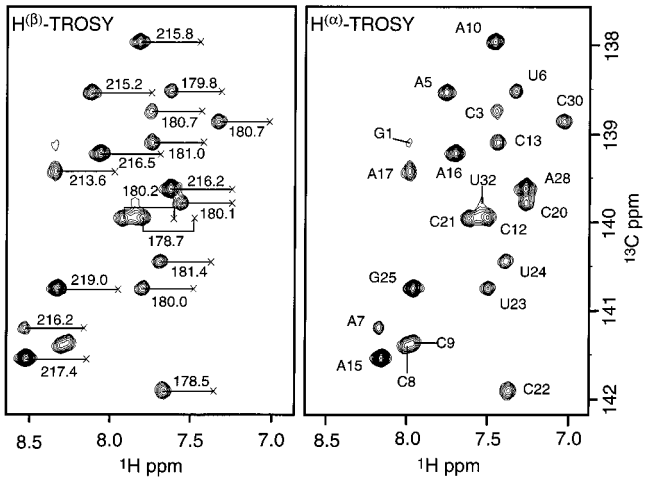


**Figure 5.** $H^{(\beta)}$- and $H^{(\alpha)}$-TROSY spectra recorded with the pulse sequences of Figure 1A on the 15% $^{13}$C-labeled 33-mer RNA−unlabeled theophylline complex at 14.1 T $B_0$ field strength. 1024 ($^1$H) × 256 ($^{13}$C) complex data points were collected, and the spectral widths in the $^1$H and $^{13}$C dimensions were set to 13 and 30 ppm, respectively. A recycle delay of 1.5 s was chosen, and the experimental time was 36 h per experiment. After multiplication with an exponential line broadening function ($\Delta\nu = 10$ Hz) in $t_1$ and a squared cosine function in $t_2$, the spectra were zero-filled and Fourier-transformed to final matrixes of 16384 × 2048 points. Only a small part of the $^1$H−$^{13}$C correlation map is displayed corresponding to the $C_6/C_8$ carbons. The C−H coupling constants were obtained from the relative peak positions of the corresponding cross-peaks in the $^1$H dimension using a fitting routine in FELIX.

**Measurement of C−H One-Bond Coupling Constants.** The recording of two experiments, a $H^{(\alpha)}$-TROSY and a $H^{(\beta)}$-TROSY allows the accurate measurement of heteronuclear C−H coupling constants from the relative peak positions of the corresponding cross-peaks in the $^1$H dimension of the 2D spectra. This is demonstrated in Figure 5 for the $C_6$ and $C_8$ base carbons of the 15% $^{13}$C-labeled RNA sample. $^1$H−$^{13}$C correlation spectra of almost the same quality in terms of sensitivity and spectral resolution are obtained for the $H^{(\alpha)}$-TROSY and $H^{(\beta)}$-TROSY, reflecting the small anisotropy of the $^1$H CSA tensor. Therefore, most of the cross-peaks are well-resolved in both spectra, and the $^1$H frequencies can be extracted with high precision.

This method for measuring heteronuclear one-bond coupling constants can be compared to other previously described techniques, mainly developed for application to proteins. In the simplest approach, a $^1$H−$^{13}$C correlation spectrum is recorded without heteronuclear decoupling in either the $^1$H or the $^{13}$C frequency dimension. For larger RNAs, this method suffers from the poor spectral resolution since there are twice as many peaks present in the spectrum. Several methods have been proposed to separate the doublet peaks, detected in the $\omega_1$ frequency dimension, in two different spectra. In the IPAP and HSQC-$\alpha/\beta$ approaches,[11,12] an additional pulse sequence element is inserted to separate the $C^{(\alpha)}$ and $C^{(\beta)}$ doublet components in different spectra. The coupling constant is then obtained from the frequency difference of $^{13}$C resonance positions. In the case of aromatic C−H spin pairs, however, this method has the problem that the $C^{(\alpha)}$ resonances are broadened by the CSA−dipolar relaxation interference as described in the previous section. For larger RNAs, severe overlap problems will occur and the sensitivity of the $C^{(\alpha)}$-selected experiment will dramatically drop. A further advantage of the $H^{(\alpha)}/H^{(\beta)}$-TROSY approach is the significantly smaller dynamic frequency shift

(29) Tegenfeldt, J.; Feucht, H.; Ruschitzka, G.; Haeberlen, U. *J. Magn. Reson.* **1980**, *39*, 509−520.
(30) (a) Allain, F. H. T.; Varani, G. *Nucleic Acids Res.* **1995**, *23*, 341−350. (b) Legault, P.; Pardi, A. *J. Am. Chem. Soc.* **1994**, *116*, 8390−8391. (c) Legault, P.; Pardi, A. *J. Am. Chem. Soc.* **1997**, *119*, 6621−6628.
(31) Oldfield, E. *J. Biomol. NMR* **1995**, *5*, 217−225.
(32) Wishart, D. S.; Sykes, B. D. *Methods Enzymol.* **1995**, *239*, 363−392.
(33) (a) Ghose, R.; Marino, J. P.; Wiberg, K. B.; Prestegard, J. H. *J. Am. Chem. Soc.* **1994**, *116*, 8827−8828. (b) Wijmenga, S. S.; Kruithof, M.; Hilbers, C. W. *J. Biomol. NMR* **1997**, *10*, 337−350.
(34) Ottiger, M.; Tjandra, N.; Bax, A. *J. Am. Chem. Soc.* **1997**, *119*, 9825−9830.

contribution[35] to the C−H splitting. As dynamic frequency shifts also originate from the interference of CSA and dipolar interactions, this effect has little influence on the splitting in the $^1H$ dimension, but in the case of aromatic carbons this leads to a non negligible systematic error in the measured coupling constants from the splittings in the $^{13}C$ frequency dimension.

Alternatively, J-modulation experiments have been proposed[36] for coupling constants measurements with very high precision. They are based on a series of CT-HSQC-type spectra and are therefore considerably less sensitive and more time-consuming. Whenever the precision obtained from the relative peak positions in 2D spectra is sufficient, the $H^{(\alpha)}/H^{(\beta)}$-TROSY method will be an attractive alternative for the measurement of C−H coupling constants in RNA.

At this time, it is difficult to relate the scalar C−H coupling constants to the local structure of the RNA molecule. An important reason for measuring one-bond C−H coupling constants in RNA is the extraction of residual dipolar coupling constants, which provides powerful structural information. In favorable cases (large anisotropic magnetic susceptibility tensors) residual dipolar couplings can be obtained from the magnetic $B_0$ field dependence of the C−H splitting. Alternatively, with the availability of liquid crystalline media added to the RNA sample,[6] a tunable degree of molecular alignment in the magnetic field is obtained, and residual C−H dipolar couplings cover a range which is much larger than the precision provided by the $H^{(\alpha)}/H^{(\beta)}$-TROSY based measurement. It is expected that dipolar coupling constants will have an increasing impact on structure calculations of larger RNAs.[6]

**Three-Dimensional $^{13}C$-Edited NOESY.** The gain in sensitivity and resolution obtained from spin-state selective $^1H-^{13}C$ correlation experiments can also be incorporated into 3D NOESY-type experiments, and Figure 1B shows the $^{13}C$-edited sensitivity-enhanced 3D TROSY-NOESY pulse sequence. A 3D data set was recorded at a magnetic field strength of 18.8 T, with the experimental details given in the captions to Figures 1 and 6. Two-dimensional slices taken at different $\omega_2$ ($^1H$) frequencies are shown in Figure 6 to illustrate the quality of the data. A high spectral resolution is obtained in the $^{13}C$ dimension, as a result of the absence of homonuclear $^{13}C-^{13}C$ splittings and the CSA−dipolar interference, allowing, for example, the clear separation of the carbon resonances of $C_2$-A15 and $C_2$-A16 or $C_6$−C12 and $C_6$−U23, which is not possible in a standard NOESY-HSQC experiment. Despite the very low concentration of $^{13}C$-labeled carbon sites (0.15 mM labeled sites in the ∼1 mM 15% $^{13}C$-labeled sample), various sequential NOEs between $H_{1'}$ and aromatic base protons and between different bases are observed in these 2D slices. Since the resonance assignment process is still mainly based on the detection of a complete set of sequential NOEs, this high resolution experiment may be crucial to solve ambiguities due to peak overlap in spectra recorded with standard techniques on fully $^{13}C$-labeled samples. Although the observed signal-to-noise ratio of the data is not yet sufficient for complete assignment, we believe that this type of high resolution NOESY spectra will be very helpful in the assignment process, and for identification of structurally relevant NOEs.

A combination of the TROSY-NOESY approach with selective deuteration techniques[4] will further improve the sensitivity and the spectral resolution of the experiment. The resolution improvement obtained by the combination of the two techniques will be especially useful in case of large RNA systems where the $^1H$ and $^{13}C$ spectra are much more crowded.

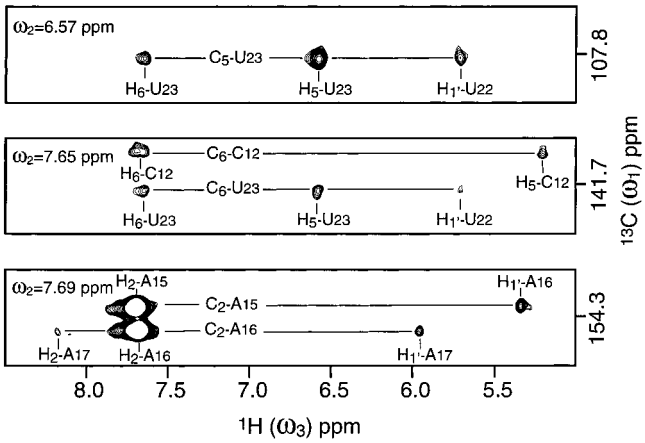


**Figure 6.** Two-dimensional strips of a 3D $H^{(\alpha)}$-TROSY-NOESY spectrum recorded on the 15% $^{13}C$-labeled 33-mer RNA at 18.8 T $B_0$ field strength. The strips show a region of individual [$^{13}C(\omega_1)$,$^1H(\omega_3)$] planes extracted at different $^1H(\omega_2)$ frequencies. The 3D data set was acquired using the pulse sequence of Figure 1B with 122 × 40 × 512 complex points, and spectral widths of 30, 5, and 13 ppm for the $^{13}C$-($\omega_1$),$^1H(\omega_2)$, $^1H(\omega_3)$ dimensions, respectively. A recycle delay of 1.5 s and a NOE mixing time of 200 ms were used. The total experimental time was 3.5 days. After apodization with an exponential line broadening ($t_3$) and squared cosine ($t_1$ and $t_2$) functions, the data were zero-filled and Fourier-transformed to a final matrix of 256 × 256 × 512 points.

## Conclusions

Spin-state selective TROSY experiments combined with fractional 15% $^{13}C$ labeling yield $^1H-^{13}C$ correlation spectra of RNA with high spectral resolution and significantly increased sensitivity. The longer spin−lattice relaxation time constants of the protons as compared to the carbons, make the TROSY approach especially attractive for RNAs. For aromatic base carbons, the enhancement effect is maximal at currently available $B_0$ field and is independent of the molecular size. Applications of this technique to a 33-mer RNA for measurement of one-bond C−H coupling constants and $^{13}C$-edited $^1H-^1H$ NOEs indicate that spin-state selective $^1H-^{13}C$ experiments will be very helpful for the resonance assignment and structure determination of larger RNAs. The experiments presented here can also be applied to unlabeled molecules at natural abundance and can be extended to fully $^{13}C$-labeled RNA using constant-time techniques, and such applications are currently being investigated.

**Acknowledgment.** This work was supported by the Commissariat à l'Energie Atomique, the Centre National de la Recherche Scientifique (exchange agreement with NSF- project No. 4380), and Molecular Simulations Inc. (San Diego, CA). A.P. acknowledges financial support from NIH Grant AI33098 and a NSF International Travel Award (INT-9602955). The 3D NOESY-TROSY data were recorded at the European Large Scale Facility in Florence, Italy. We also thank Analisa Brown for preparation of the 15% $^{13}C$-labeled RNA. This is publication no. 559 of the IBS - J.P. Ebel.

JA982853L

(35) (a) Werbelow, L. G. *J. Chem. Phys.* **1979**, *70*, 5381−5383. (b) Brüschweiler, R. *Chem. Phys. Lett.* **1996**, *257*, 119−122.

(36) Tjandra, N.; Grzesiek, S.; Bax, A. *J. Am. Chem. Soc.* **1996**, *118*, 6264−6272.

(37) Marion, D.; Ikura, M.; Tschudin, R.; Bax, A. *J. Magn. Reson.* **1989**, *85*, 393−399.